Moment-based formulation of Navier–Maxwell slip boundary conditions for lattice Boltzmann simulations of rarefied flows in microchannels

Tim Reis[1] and Paul J. Dellar[1]
Oxford Centre for Collaborative Applied Mathematics
Mathematical Institute, 24–29 St Giles', OX1 3LB, United Kingdom[a)]

We present an implementation of first-order Navier–Maxwell slip boundary conditions for simulating near-continuum rarefied flows in microchannels with the lattice Boltzmann method. Rather than imposing boundary conditions directly on the particle velocity distribution functions, following the existing discrete analogs of the specular and diffuse reflection conditions from continuous kinetic theory, we use a moment-based method to impose the Navier–Maxwell slip boundary conditions that relate the velocity and the strain rate at the boundary. We use these conditions to solve for the unknown distribution functions that propagate into the domain across the boundary. We achieve second-order accuracy by reformulating these conditions for the second set of distribution functions that arise in the derivation of the lattice Boltzmann method by an integration along characteristics. The results are in excellent agreement with asymptotic solutions of the compressible Navier-Stokes equations for microchannel flows in the slip regime. Our moment formalism is also valuable for analysing the existing boundary conditions, and explains the origin of numerical slip in the bounce-back and other common boundary conditions that impose explicit conditions on the higher moments instead of on the local tangential velocity.

I. INTRODUCTION

Small-scale hydrodynamics (microfluidics) has generated significant interest in recent years due to technological advancements in micro-electro-mechanical-systems (MEMS), and their rapidly increasing number of application areas.[1–4] Microfluidic devices are characterised by small length-scales L that become comparable with the molecular mean free path λ. The relevance of the Navier–Stokes equations, derived as an asymptotic expansion for small Knudsen number, $Kn = \lambda/L \ll 1$, thus becomes questionable for describing flows in these devices. However, the flow regimes differ very substantially from hypersonic flows, the traditional focus of rarefied gas dynamics.[5]

Microdevices typically operate in the isothermal slip-flow regime, characterised by $0.01 \lesssim Kn \lesssim 0.1$, and a Mach number $Ma = |\mathbf{u}|/c_s \ll 1$. The fluid velocity $\mathbf{u}$ is thus substantially smaller than the sound speed c_s, but substantial density variations typically still occur through a balance between pressure gradients and viscosity. The Navier–Stokes equations remain valid in the bulk of the flow, but they must be supplemented by suitable slip boundary conditions. Sone[6] has identified an asymptotic regime governed by the Stokes equations with second-order slip boundary conditions, and Hadjiconstantinou[7] has shown that the Navier–Stokes equations with second-order slip boundary conditions describe flow in microchannels up to $Kn \sim 1$. These boundary conditions may be derived from kinetic theory using the method of matched asymptotic expansions (see Sec. II).

Rarefied monatomic gases are described by the Boltzmann equation[8–11]

$$\partial_t f + \mathbf{c} \cdot \nabla f = C[f, f]. \tag{1}$$

The distribution function $f(\mathbf{x}, \mathbf{c}, t)$ gives the number density of particles moving with velocity $\mathbf{c}$ at position $\mathbf{x}$ and time t, and $C[f, f]$ denotes Boltzmann's binary collision operator. A widely used boundary condition, introduced by Maxwell,[12] expresses the distribution of particles moving away from the boundary ($\mathbf{c} \cdot \mathbf{n} > 0$) as[13,14]

$$f(\mathbf{x}, \mathbf{c}, t) = (1 - \alpha) f(\mathbf{x}, \mathbf{c} - 2\mathbf{n}\,\mathbf{n} \cdot \mathbf{c}, t) + \alpha f^{(0)}_{wall}(\mathbf{x}, \mathbf{c}, t) \text{ for } \mathbf{c} \cdot \mathbf{n} > 0. \tag{2}$$

The first term represents specular reflection, reversing the sign of the normal component of the particle velocity, and the second represents diffuse reflection, *i.e.* re-emission of particles with a Maxwell–Boltmzann distribution $f^{(0)}_{wall}$ for the temperature and velocity of the wall, and a density chosen to give zero mass flux through the wall. The outgoing distribution is thus a blend of specular and diffuse reflection, as set by an accommodation coefficient α that typically between 0.8 and 1 for most solid materials.[3,15]

The lattice Boltzmann method approximates the continuous Boltzmann equation (1) by restricting the particle velocity $\mathbf{c}$ to a discrete set $\mathbf{c}_0, \ldots, \mathbf{c}_{N-1}$. The most commonly used discrete set, known as D2Q9, uses nine velocities arranged on a square lattice, as shown in figure 1. The lattice Boltzmann method is now well-established as a computational technique for solving the Navier–Stokes equations, so it is natural to enquire whether its kinetic heritage offers advantages for computing rarefied flows. This question has received a lot of attention, with the vast majority of work adapting Maxwell's combination (2) of diffuse and specular reflection to a discrete velocity space.[16–24]

However, the standard lattice Boltzmann method is restricted to capturing just the first few moments of the solutions of the true Boltzmann equation (see Sec. IV C). One is thus essentially computing solutions to the Navier–Stokes

a)Electronic mail: [reis,dellar]@maths.ox.ac.uk

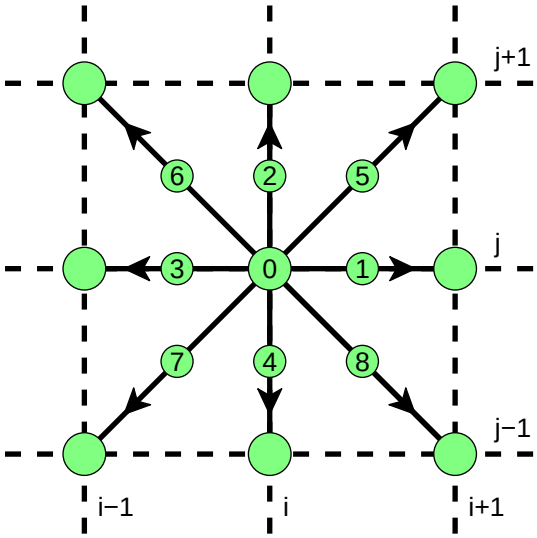

FIG. 1. (Color online) The nine particle propagation velocities $\mathbf{c}_0, \ldots, \mathbf{c}_8$ in the D2Q9 integer lattice.

equations, but with a Knudsen number appreciably larger than zero. He *et al.*[25] have shown that the D2Q9 lattice Boltzmann method for shear flow reduces to a linear second-order recurrence relation for the streamwise velocity. Solutions to this recurrence relation thus give linear or parabolic profiles at all Knudsen numbers, as in the exact solutions of the Navier–Stokes equations. The D2Q9 lattice Boltzmann method therefore cannot capture the kinetic boundary layers, or Knudsen layers, that appear in solutions of the Boltzmann equation near solid boundaries. The Knudsen layers are essential for transforming the boundary conditions (2) into effective boundary conditions for the Navier–Stokes equations that describe flow in the interior, as shown in Sec. II and figure 2 below.

In this paper we address the more modest goal of implementing the Navier–Maxwell slip boundary conditions for the Navier–Stokes equations in the slip flow regime. In a departure from previous work, we do not pursue the analogy with Maxwell's boundary condition (2) for the Boltzmann equation to formulate boundary conditions on the discrete distribution functions. Instead, we use the moment approach of Bennett[26,27] to apply boundary conditions directly to hydrodynamic quantities, the velocity and momentum flux. We are thus able to reproduce asymptotic solutions of the Navier–Stokes equations with Navier–Maxwell boundary conditions. We do not address the extent to which the missing Knudsen layers may be satisfactorily modelled by an imposed a spatially varying viscosity near walls,[28,29] except to note that numerical evidence suggests that the tangential velocity in the Knudsen layers follows a power law of the form $u(y) = u(0) + Cy^\alpha$ with $\alpha < 1$. The tangential velocity gradient is singular at the wall, so the effective viscosity must be zero.[30].

The applicability of the lattice Boltzmann method to the slip-flow regime is made more complicated by the existence of a purely numerical slip in the widely used combination of bounce-back boundary conditions and the Bhatnagar–Gross–Krook or BGK collision operator.[24,25,31,32] The precise point at which the velocity tangential to a boundary vanishes depends upon the Knudsen number, and only asymptotes to half-way between grid points as $Kn \to 0$. Simulations of rarefied flow using bounce-back boundary conditions and the BGK collision operator therefore suffer from a resolution-dependent numerical slip in addition to the intended slip. Verhaeghe *et al.*[24] have offered a detailed critique of existing lattice Boltzmann formulations for slip flow based on the BGK collision operator and kinetic boundary conditions, following the observations of Shen *et al.*[33] Moreover, the Knudsen layers in the true Boltzmann solution occupy an $\mathcal{O}(Kn)$-wide region where the fluid velocity is itself $\mathcal{O}(Kn)$, as shown in figure 2, so they contribute $\mathcal{O}(Kn^2)$ to the total volume flux. Obtaining a satisfactory volume flux thus does not imply correctness of the computed flow field.[7]

II. THE SLIP-FLOW REGIME AND KRAMERS' PROBLEM

The slip-flow regime is best illustrated by Kramers' problem for linear shear flow over an infinite flat plate.[9,11,34,35] Using the BGK[31] collision operator for simplicity, Kramers' problem for a plate is located at $y = 0$ may be formulated as the integral equation[36–38]

$$v\partial_y Y + Y(y,v) = \pi^{1/2} \int_0^\infty \exp(-c^2) Y(y,c)\, dc, \tag{3}$$

and solved analytically using integral transforms. The velocity field may be written as[10,38]

$$u(y) = a\lambda \left[\frac{y}{\lambda} + A - U_d\left(\frac{y}{\lambda}\right) \right], \tag{4}$$

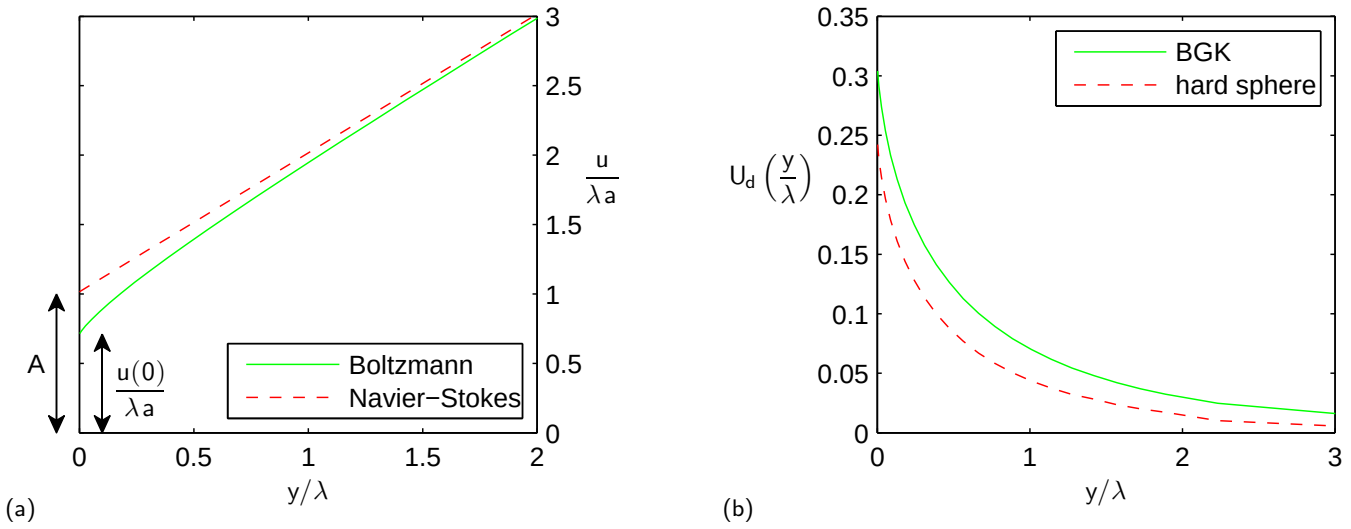

FIG. 2. (Color online) (a) The Knudsen layer and slip velocity in Kramers' problem. The slip velocity $u_{slip} = 1.01615\lambda a$ that must be applied to the Navier–Stokes equations to match the flow in the core (where $y \gg \lambda$) is larger than the true tangential velocity $u(0) = \lambda a/\sqrt{2}$ at the wall. (b) The velocity defect function $U_d(y/\lambda)$ from numerical quadratures for the BGK and hard-sphere collision operators.[38]

where the constant a specifies the strength of the shear at infinity, and $\lambda = \mu\sqrt{2RT}/p$ defines the mean free path. The function $U_d(y/\lambda)$ is called the velocity defect. It decays rapidly to zero for $y \gg \lambda$, leaving a linear shear flow offset by an amount $A\lambda$. This slip coefficient is $A = 1.01615$ for a purely diffusive wall ($\alpha = 1$) with the BGK collision operator, and about 3% smaller for more realistic collision operators.[4,9,39] A direct evaluation gives $u(0) = \lambda a/\sqrt{2}$ for the tangential velocity at the wall. This is substantially smaller than the apparent slip velocity $1.01615\lambda a$ seen in the far field. Figure 2 shows the full solution $u(y)$ and the velocity defect function $U_d(y/\lambda)$ computed using numerical quadratures for the BGK and hard-sphere collision operators.[38]

More generally, the solution of Kramers' problem describes the flow in an $\mathcal{O}(\lambda)$-wide Knudsen boundary layer close to a wall. It thus provides the inner solution in a small Kn approximation to general flow problems based on matched asymptotic expansions,[5,9,13,40,41] in which the Knudsen layers are captured using a boundary-layer scaling of the wall-normal coordinate, $y = Kn\,Y$ with $Y = \mathcal{O}(1)$. The Knudsen layers may be intepreted as the regions of physical space over which collisions smooth away the discontinuities of the distribution function in velocity space created by the boundary conditions.[13]

The flow outside the Knudsen layer may be captured by the Navier–Stokes equations with slip boundary conditions, usually written as[4]

$$u_{\parallel} = \tilde{\sigma}\lambda\frac{\partial u_{\parallel}}{\partial n} \tag{5}$$

in terms of the normal derivative of the tangential velocity $u_{\parallel}$ at the wall. The constant $\tilde{\sigma} = (2-\alpha)/\alpha$ is sometimes called the streamwise momentum accommodation coefficient, while the α appearing in (2) is called the tangential momentum accommodation coefficient. The boundary condition (5) gives the exact solution for Kramers' problem outside the Knudsen layer if we take $\tilde{\sigma} = A = 1.01615$. A more general condition, valid at curved boundaries, may be formulated using the momentum flux tensor at the wall,[42]

$$\mathbf{u}_{\parallel} = \mathbf{u}\cdot(\mathsf{I}-\mathbf{nn}) = -\frac{\tilde{\sigma}\lambda}{\mu}\mathbf{n}\cdot\mathbf{\Pi}^{visc}\cdot(\mathsf{I}-\mathbf{nn}), \tag{6}$$

where μ is the dynamic viscosity, $\mathbf{\Pi}^{visc}$ is the viscous momentum flux, and $\mathbf{n}$ is a unit vector normal to the boundary. The tensor $\mathsf{I}-\mathbf{nn}$ projects vectors onto their components tangential to the boundary. This is the form given by Maxwell,[12] and earlier still by Navier.[43,44] The tensorial expression (6) may be derived from Maxwell's kinetic boundary condition (2) by evaluating half-range moments over $\mathbf{c}\cdot\mathbf{n} \gtrless 0$ of the expression for the distribution function at the wall given by the Chapman–Enskog expansion.[13]

In this paper we construct a lattice Boltzmann implementation of the macroscopic Navier–Maxwell slip boundary condition (6). We use the approach of Bennett[26,27] to apply boundary conditions directly to hydrodynamic quantities, the velocity and momentum flux. Bennett's approach was originally used to impose no-slip boundary conditions on multi-component mixtures, in which the individual species may slip relative to the boundary.[26,27] It has since been used to construct no-slip boundary conditions for single-component fluids that impose a zero velocity boundary precisely at lattice points, irrespective of the collision operator used. The moment approach is also instructive for analysing existing boundary conditions for the distribution functions, such as bounce-back and specular or diffuse reflection (see section V C).

III. NAVIER–STOKES THEORY FOR FLOW IN A MICROCHANNEL

We consider a viscous fluid flowing through a microchannel of length L and height H, such that the aspect ratio $\delta = H/L \ll 1$. The flow is characterised by three dimensionless parameters, the Reynolds number, the Mach number, and the Knudsen number, which we define to be

$$Re = \frac{\bar{\rho}_o \bar{u}_o H}{\mu}, \quad Ma = \frac{\bar{u}_o}{\sqrt{\gamma R T}}, \quad Kn = \sqrt{\frac{\pi\gamma}{2}}\frac{Ma}{Re}. \tag{7}$$

Here, $\bar{\rho}_o$ and $\bar{u}_o$ are the average density and velocity at the outlet, μ is the (constant) dynamic viscosity, $\gamma = 5/3$ is the ratio of specific heats for an ideal monatomic gas, T is the temperature, and R the gas constant.

The last equality in (7) expresses the von Kármán relation between the three dimensionless parameters.[3,4,45] However, this particular choice of constants corresponds to a mean free path $\ell = KnH = \lambda\sqrt{\pi}/2$ in the notation of Cercignani.[10] These two forms ℓ and λ are widely used in the literature. Boltzmann's binary collision operator defines a collision frequency $\nu(c)$ that depends upon the particle velocity, so there is no universally accepted definition of mean free path. As we used λ rather than ℓ to formulate Kramers' problem in Sec. II, the slip coefficient σ used in the Navier–Stokes theory for the remainder of this paper differs by a factor of $2/\sqrt{\pi}$ from the $\tilde{\sigma}$ used in Sec. II.

To comply with restrictions on the validity of the lattice Boltzmann equation (see section IV), we consider low Mach number ($Ma \ll 1$) and collision-dominated ($Kn \ll 1$) isothermal flows. The isothermal approximation is valid for flow in long, uninsulated microchannels at small Mach numbers.[45] We rewrite the Navier–Maxwell slip boundary condition (5) for planar boundaries as

$$u|_{wall} = \sigma KnH \left.\frac{\partial u}{\partial y}\right|_{wall}, \tag{8}$$

where KnH now defines the mean free path, and σ defines the corresponding streamwise momentum accommodation coefficient. We non-dimensionalise the steady-state, isothermal, compressible Navier-Stokes equations using a horizontal coordinate $\hat{x} = x/L \in [0,1]$ and a vertical coordinate $\hat{y} = y/H \in [-1/2, 1/2]$. An expansion in $\delta = H/L \ll 1$ gives the leading-order solution[4,45]

$$\hat{u}(\hat{x},\hat{y}) = -\frac{\delta Re}{8\gamma Ma^2}\frac{d\hat{p}}{d\hat{x}}\left(1 - 4\hat{y}^2 + 4Kn\frac{\sigma}{\hat{p}}\right), \tag{9a}$$

$$\hat{v}(\hat{x},\hat{y}) = \frac{\delta^2 Re}{8\gamma\hat{p}Ma^2}\left[\frac{1}{2}\frac{d^2(\hat{p}^2)}{d\hat{x}^2}\left(1 - \frac{4}{3}\hat{y}^2\right) + 4\,\sigma Kn\frac{d^2\hat{p}}{d\hat{x}^2}\right]\hat{y}, \tag{9b}$$

$$\hat{p}(\hat{x}) = \Big[(6\sigma Kn)^2 + (1 + 12\sigma Kn)\hat{x} + \theta(\theta + 12\sigma Kn)(1 - \hat{x})\Big]^{1/2} - 6\,\sigma Kn, \tag{9c}$$

where $\hat{u} = u/\bar{u}_o$, $\hat{v} = v/\bar{u}_o$, $\hat{p} = p/p_o$, $\theta = \bar{p}_i/\bar{p}_o$, and $\bar{p}_i$ and $\bar{p}_o$ are the average pressures at the inlet and outlet, respectively.

The solution (9a) is a parabolic profile, like the standard Poiseuille flow solution for no-slip boundary conditions, but shifted by an $\mathcal{O}(Kn)$ amount $4\sigma Kn/\hat{p}$ due to the slip boundary conditions. This shift vanishes as $Kn \to 0$, for which the boundary condition (8) reduces to the usual non-slip condition. The cross-channel (spanwise) velocity $\hat{v}$ is not zero, as for standard Poiseuille flow, but instead has a cubic profile in $\hat{y}$. The spanwise velocity is, however, $\mathcal{O}(\delta)$ smaller than the streamwise velocity $\hat{u}$, as required to satisfy mass conservation. The pressure $\hat{p}(\hat{x})$ is uniform across the channel, as is usual under the boundary layer scaling when $\delta = H/L \ll 1$. However, the pressure gradient $d\hat{p}/d\hat{x}$ is not uniform, as in standard Poiseuille flow, but instead varies with $\hat{x}$.

IV. THE LATTICE BOLTZMANN METHOD

In this section we briefly outline the popular D2Q9 lattice Boltzmann model.[46] We begin with the discrete Boltzmann equation for the evolution of a set of particle distribution functions $f_i(\mathbf{x}, t)$,

$$\frac{\partial f_i}{\partial t} + \mathbf{c}_i \cdot \nabla f_i = -\frac{1}{\tau}\left(f_i - f_i^{(0)}\right), \quad \text{for } i = 0, \ldots, N-1. \tag{10}$$

Each f_i advects with the corresponding particle velocity $\mathbf{c}_i$. The $\mathbf{c}_i$ are chosen to form a square lattice in the D2Q9 model (see figure 1). It is convenient to adopt the so-called lattice units in which $|\mathbf{c}_{1,\ldots,4}| = 1$ and $|\mathbf{c}_{5,\ldots,8}| = \sqrt{2}$. The $\mathbf{c}_i$ then form an integer lattice in velocity space.

The BGK[31] collision operator on the right hand side of (10) relaxes the f_i towards the equilibria[46]

$$f_i^{(0)} = w_i \rho\left(1 + 3\mathbf{c}_i \cdot \mathbf{u} + \frac{9}{2}(\mathbf{c}_i \cdot \mathbf{u})^2 - \frac{3}{2}|\mathbf{u}|^2\right), \tag{11}$$

with a single relaxation time τ. These equilibria are functions of the macroscopic density ρ and velocity $\mathbf{u}$, as defined in (13) below. The equation of state is $p = \rho/3$, so $c_s^2 = 1/3$ in lattice units. In other words, the sound speed is $1/\sqrt{3}$ of the speed of the particles moving along the axes of the lattice.

The weights w_i are

$$w_i = \begin{cases} 4/9, & i = 0, \\ 1/9, & i = 1, 2, 3, 4, \\ 1/36, & i = 5, 6, 7, 8. \end{cases} \tag{12}$$

These weights, and the discrete velocities $\mathbf{c}_i$, correspond to a Gauss–Hermite quadrature in velocity space.[47,48] The equilibria (11) may thus be derived from an expansion of the continuous Maxwell–Boltzmann distribution up to second order in Mach number.[47,48] More generally, the lattice Boltzmann approach produces a low order polynomial in $\mathbf{c}$ approximation to the behavior of the continuous distribution function $f(\mathbf{x}, \mathbf{c}, t)$ under the Boltzmann equation.

Hydrodynamic quantities, such as the density ρ, momentum $\rho\mathbf{u}$, and momentum flux $\mathbf{\Pi}$, are defined by moments of the f_i with respect to the particle velocities,

$$\rho = \sum_i f_i, \quad \rho\mathbf{u} = \sum_i f_i \mathbf{c}_i, \quad \mathbf{\Pi} = \sum_i f_i \mathbf{c}_i \mathbf{c}_i, \quad \boldsymbol{Q} = \sum_i f_i \mathbf{c}_i \mathbf{c}_i \mathbf{c}_i. \tag{13}$$

The corresponding moments of the discrete Boltzmann equation (10) give the evolution equations

$$\partial_t \rho + \nabla \cdot (\rho\mathbf{u}) = 0, \tag{14a}$$

$$\partial_t (\rho\mathbf{u}) + \nabla \cdot \mathbf{\Pi} = 0, \tag{14b}$$

$$\partial_t \mathbf{\Pi} + \nabla \cdot \boldsymbol{Q} = -\frac{1}{\tau} \left(\mathbf{\Pi} - \mathbf{\Pi}^{(0)} \right). \tag{14c}$$

The first two right hand sides vanish because the collision term conserve mass and momentum, while the momentum flux relaxes towards equilibrium on the collisional timescale τ. Exactly the same system of moment equations may be obtained from integral moments of the continuous Boltzmann equation using Maxwell's equation of transfer.[8,9,11] The right hand side of (14c) then follows from the linearised Boltzmann collision operator for Maxwell molecules, and from many model collision operators such as BGK.[31]

The BGK collision operator on the right hand side of (10) is just the simplest example that leads to the desired moment system (14a)-(14c). More generally, we may consider the discrete Boltzmann equation

$$\frac{\partial f_i}{\partial t} + \mathbf{c}_i \cdot \nabla f_i = -\sum_j \Omega_{ij} \left(f_j - f_j^{(0)} \right), \tag{15}$$

with a constant collision matrix Ω_{ij}. The BGK collision operator corresponds to choosing $\Omega_{ij} = \tau^{-1}\delta_{ij}$, but other choices lead to improvements in both numerical stability[49–51] and the treatment of boundary conditions. The two-relaxation-time (TRT) collision operator applies different relaxation times to the odd and even moments of the f_i, and in particular for $\mathbf{\Pi}$ and $\boldsymbol{Q}$. Imposing the so-called "magic" relation $\tau_Q = 3/(16\tau_\Pi)$ between these two relaxation times fixes the location of the effective boundary for bounce-back boundary conditions to be precisely half-way between grid points, independent of the value of the momentum flux relaxation time τ.[52,53]

A. Macroscopic limit

As in continuous kinetic theory, we derive the Navier–Stokes equations by seeking solutions of (10), solutions that vary slowly over timescales much longer than the collision time τ.[8,9,11] We introduce a small parameter ϵ, which may be identified with the Knudsen number Kn, into the collision time by replacing τ with $\epsilon\tau$. Using the multiple-scales form of the Chapman–Enskog expansion, we then expand the non-conserved moments $\mathbf{\Pi}$ and $\boldsymbol{Q}$, and the time derivative, as series in ϵ,

$$\mathbf{\Pi} = \mathbf{\Pi}^{(0)} + \epsilon\mathbf{\Pi}^{(1)} + \cdots, \quad \boldsymbol{Q} = \boldsymbol{Q}^{(0)} + \epsilon\boldsymbol{Q}^{(1)} + \cdots, \quad \partial_t = \partial_{t_0} + \epsilon\partial_{t_1} + \cdots. \tag{16}$$

The conserved moments ρ and $\mathbf{u}$ are left unexpanded. The expansion of the time derivative is necessary to suppress secular terms that would otherwise disorder the expansion on long timescales $t = \mathcal{O}(1/\epsilon)$. One may think of $t_0 \sim t$ and $t_1 \sim \epsilon t$ as characteristic timescales for advection and viscous diffusion respectively.

Substituting these expansions into the moment system (14a)-(14c) and neglecting terms of $\mathcal{O}(\epsilon^2)$ and above yields the isothermal compressible Navier-Stokes equations,

$$\partial_t \rho + \nabla \cdot (\rho\mathbf{u}) = 0, \tag{17}$$

$$\partial_t (\rho\mathbf{u}) + \nabla \cdot \left(\mathbf{\Pi}^{(0)} + \tau\mathbf{\Pi}^{(1)} \right) = 0, \tag{18}$$

where

$$\mathbf{\Pi}^{(0)} = \frac{\rho}{3}\mathsf{I} + \rho\mathbf{u}\mathbf{u}, \quad \mathbf{\Pi}^{(1)} = -\frac{\rho}{3}\left(\nabla\mathbf{u} + (\nabla\mathbf{u})^\mathsf{T} \right) + \mathcal{O}(Ma^3). \tag{19}$$

The second of equations (19) is derived from the leading-order approximation to (14c) under the multiple-scales expansion,

$$\partial_{t_0}\mathbf{\Pi}^{(0)} + \nabla\cdot\boldsymbol{Q}^{(0)} = -\frac{1}{\tau}\mathbf{\Pi}^{(1)}, \tag{20}$$

by evaluating $\partial_{t_0}\mathbf{\Pi}^{(0)}$ using the Euler equations. Neglecting the $\mathcal{O}(Ma^3)$ error in the viscous stress, these are the Navier–Stokes equations for an isothermal fluid with equation of state $p = \rho/3$ and dynamic viscosity $\mu = \tau\rho/3$.

B. Reduction to fully discrete form

To solve (10) numerically we must further discretise it in space and time. We integrate (10) along a characteristic for time Δt to obtain

$$f_i(\mathbf{x}+\mathbf{c}_i\Delta t, t+\Delta t) - f_i(\mathbf{x},t) = \int_0^{\Delta t} \mathcal{C}_i(x+c_i s, t+s)ds, \tag{21}$$

where $\mathcal{C}_i$ represents the collision operator on the right-hand side of (10). The left hand side of (10) is a derivative along a characteristic, so the left hand side of (21) is *exact*. We approximate the remaining integral (21) by the trapezium rule to yield a second-order accurate but *implicit* system of algebraic equations,

$$f_i(\mathbf{x}+\mathbf{c}_i\Delta t, t+\Delta t) - f_i(\mathbf{x},t) = \frac{\Delta t}{2}\Big(\mathcal{C}_i(\mathbf{x}+\mathbf{c}_i\Delta t, t+\Delta t) + \mathcal{C}_i(\mathbf{x},t)\Big) + \mathcal{O}\left(\Delta t^3\right). \tag{22}$$

Following He *et al.*[54] we now introduce the change of variables

$$\bar{f}_i\left(\mathbf{x}',t'\right) = f_i\left(\mathbf{x}',t'\right) + \frac{\Delta t}{2\tau}\left(f_i\left(\mathbf{x}',t'\right) - f_i^{(0)}\left(\mathbf{x}',t'\right)\right). \tag{23}$$

Using these variables, the previous implicit scheme (22) rearranges into explicit formulae for the $\bar{f}_i$ at the new timestep,

$$\overline{f}_i(\mathbf{x}+\mathbf{c}_i\Delta t, t+\Delta t) - \overline{f}_i(\mathbf{x},t) = -\frac{\Delta t}{\tau+\Delta t/2}\left(\overline{f}_i(\mathbf{x},t) - f_i^{(0)}(\mathbf{x},t)\right). \tag{24}$$

We thus discard the f_i and evolve the $\bar{f}_i$ instead using (24). Density and momentum are conserved by collisions, so they may be obtained directly from moments of the $\overline{f}_i$,

$$\rho = \sum_i f_i = \sum_i \overline{f}_i, \quad \rho\mathbf{u} = \sum_i f_i\mathbf{c}_i = \sum_i \overline{f}_i\mathbf{c}_i. \tag{25}$$

Corresponding expressions for non-conserved moments must be found by taking moments of the transformation (23). For example, the momentum flux tensor is[55]

$$\mathbf{\Pi} = \frac{2\tau\overline{\mathbf{\Pi}} + \Delta t\,\mathbf{\Pi}^{(0)}}{2\tau+\Delta t} \tag{26}$$

where $\overline{\mathbf{\Pi}} = \sum_i \overline{f}_i\mathbf{c}_i\mathbf{c}_i$. We will need $\mathbf{\Pi}$ to formulate slip boundary conditions in Section V.

C. Comparison between continuous, discrete, and lattice Boltzmann equations

We conclude section IV with some remarks on the applicability of the D2Q9 lattice Boltzmann method to rarefied flows with finite Knudsen numbers. The continuous Boltzmann equation yields an infinite hierarchy of moment equations. The first three of these, (14a) to (14c), suffice for recovering the isothermal Navier–Stokes equations, but proceeding further in the Chapman–Enskog expansion introduces higher moments. For example, the $\mathcal{O}(Kn^2)$ Burnett contribution to the momentum flux is determined by

$$\frac{\partial\mathbf{\Pi}^{(0)}}{\partial t_1} + \frac{\partial\mathbf{\Pi}^{(1)}}{\partial t_0} + \nabla\cdot\boldsymbol{Q}^{(1)} = -\frac{1}{\tau}\mathbf{\Pi}^{(2)}, \tag{27}$$

and to compute $\boldsymbol{Q}^{(1)}$ we need the evolution equation for $\boldsymbol{Q}$ that itself contains the next higher moment $\boldsymbol{R} = \sum_i f_i\mathbf{c}_i\mathbf{c}_i\mathbf{c}_i\mathbf{c}_i$. These higher moments are not captured correctly by the D2Q9 lattice Boltzmann model, which contains only the nine independent moments

$$\rho, \rho u_x, \rho u_y, \Pi_{xx}, \Pi_{xy}, \Pi_{yy}, Q_{xxy}, Q_{xyy}, R_{xxyy}. \tag{28}$$

All higher moments may be expressed in terms of these nine using the relations $c_{i\alpha}^p c_{i\beta}^q = c_{i\alpha}^{p+2n} c_{i\beta}^{q+2n}$ for $p,q,n = 0,1,\ldots$. For example, $Q_{xxx} = \rho u_x$ and $Q_{yyy} = \rho u_y$ since $c_{ix}^3 = c_{ix}$ and $c_{iy}^3 = c_{iy}$. This enforced relation between

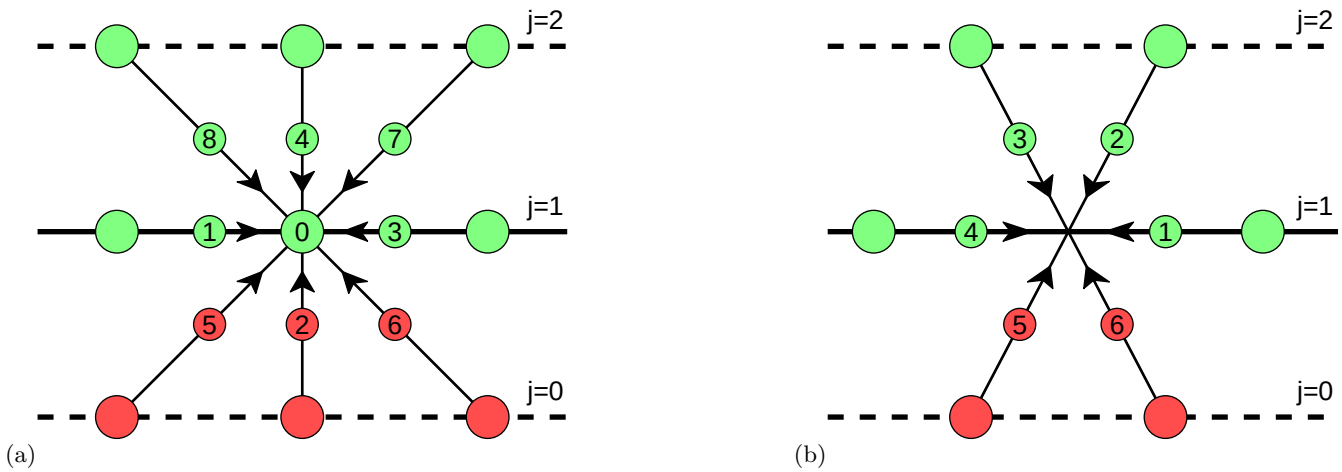

FIG. 3. (Color online) The *pre*-collisional states at a point on the southern boundary at $j = 1$. The red lattice points on the line $j = 0$ outside the boundary are missing. (a) The three missing distribution functions f_2, f_5, f_6 for the D2Q9 lattice, and (b) the two missing distribution functions f_5, f_6 for the hexagonal lattice used by Noble *et al.*[56]

these components of the $\boldsymbol{Q}$ tensor and the lower moments is responsible for the $\mathcal{O}(Ma^3)$ error in the viscous stress (19). The corresponding moment $\boldsymbol{Q}^{(0)}$ of the Maxwell–Boltzmann distribution in continuous kinetic theory contains an additional $\rho\mathbf{uuu}$ term that cancels the $\mathcal{O}(Ma^3)$ error. The incorrect equilibrium forms for $\boldsymbol{Q}$ and $\boldsymbol{R}$ in the D2Q9 lattice Boltzmann formulation also cause errors in the Burnett terms at $\mathcal{O}(Kn^2)$.

In addition, the BGK collision operator with a fixed collision time τ gives a dynamic viscosity $\mu = \tau\rho c_s^2$ proportional to ρ. By contrast, the dynamic viscosity of a real monatomic gas is independent of density, as is found from using Boltzmann's binary collision operator $C[f, f]$. Lowering the density increases the mean free path by an amount that exactly compensates for the reduced momentum transport in a lower density gas. To reproduce this effect we adjust the collision time τ to be inversely proportional to the local density at each lattice point.[55] This change does not alter the analysis that led to the second-order discretisation in Sec. IV B.

Finally, our derivation above separates the two questions of the approximation of the Navier–Stokes equations by the discrete Boltzmann partial differential equation (PDE), and the approximation of the latter PDE by the numerical scheme (24) that is the lattice Boltzmann equation. The accuracy of the former approximation is controlled by the collision time τ, while the accuracy of the latter approximation is controlled by the timestep Δt and grid spacing Δx. In principle, these are two independent parameters controlling the two independent sources of error in the approximations that link the Navier–Stokes and lattice Boltzmann equations. There is no fixed relation between the mean free path $\ell = \sqrt{\pi/2}\,\tau c_s$, as set by τ, and the grid spacing Δx.

V. MOMENT-BASED BOUNDARY CONDITIONS FOR NAVIER–MAXWELL SLIP

After each propagation step, the lattice points on the boundary contain unknown values for the distribution functions whose particle velocities point into the fluid. There are no points outside the boundary for this information to propagate in from. For example, figure 3 shows that f_2, f_5 and f_6 are unknown on the southern boundary after each propagation step. The common lattice Boltzmann boundary conditions, such as bounce-back, specify the values of the individual distribution functions. This is a natural approach in kinetic theory, analogous to Maxwell's[12] specification (2) of the incoming part of the continuous distribution function through a combination of diffuse and specular reflection. However, in discrete kinetic theory we have an invertible relation between the f_i and a finite set of moments. This suggests an alternative approach of specifying boundary conditions directly on the moments, as proposed by Bennett.[26,27] In a related earlier work, Noble *et al.*[56] determined boundary conditions for the two incoming distributions on the hexagonal lattice shown in Figure 3(b) by imposing conditions on the two components of velocity at the wall. Extending this approach to the three incoming distribution functions on the D2Q9 square lattice shown in Figure 3(a) requires an additional boundary condition.

A. Solid boundaries

We first consider a solid wall at the south of the computational domain, as shown in Figure 3(a). After propagation there are three unknowns, f_2, f_5 and f_6. We look at how these unknown quantities appear in the moments at the wall. For example, the zeroth-order moment (density) at the southern boundary may be written as $\rho = f_2 + f_5 + f_6 + (f_0 + f_1 + f_3 + f_4 + f_7 + f_8)$, where the bracketed f_i are all known quantities. The D2Q9 lattice has 9 independent moments, as listed in (28). Table I shows which combinations of the three unknowns f_2, f_5, f_6 appear in each of these 9 moments on the southern boundary.

Moments	Combination of unknowns
ρ, ρu_y, Π_{yy}	$f_2 + f_5 + f_6$
ρu_x, Π_{xy}, Q_{xyy}	$f_5 - f_6$
Π_{xx}, Q_{xxy}, R_{xxyy}	$f_5 + f_6$

TABLE I. Moment groups at the southern boundary

We may determine the three unknowns from the solution of three linearly independent conditions on the moments. In other words, we may choose one moment from each of the three rows of Table I, impose a boundary condition on these three moments, and then solve for f_2, f_5, f_6. It is natural to choose the moments that correspond to the hydrodynamic quantities: density, momentum, and momentum flux, rather than the higher-order moments $\boldsymbol{Q}$ and $\boldsymbol{R}$. In particular, it is natural to impose conditions on both components of the velocity at the wall. Surprisingly, many popular kinetic boundary conditions do not impose an explicit condition on the tangential velocity (see section V C). Lastly we impose a condition on Π_{xx}, the only member of the third group in Table I with a direct physical intepretation.

It is convenient to formulate the boundary conditions in lattice units, in which $\Delta x = \Delta t = 1$. The three conditions on the moments are then

$$\rho u_y = 0, \tag{29a}$$

$$\rho u_x = -\frac{\sigma \rho K n H\, \Pi_{xy}}{\mu} = -\sigma\sqrt{\frac{3\pi}{2}}\Pi_{xy}, \tag{29b}$$

$$\Pi_{xx} = \Pi^{(0)}_{xx} = \rho/3 + \rho u_x^2. \tag{29c}$$

We have used the equation of state $P = c_s^2\rho = \rho/3$ in lattice units to evaluate $\mathbf{\Pi}^{(0)}_{xx}$ on the right hand side of (29c), and to simplify the coefficient multiplying Π_{xy} in (29b). The condition on ρu_x follows from the xy component of the tensorial Navier–Maxwell slip boundary condition (6). The xy component of the equilibrium momentum flux vanishes on the wall, $\Pi^{(0)}_{xy} = \rho u_x u_y = 0$ using the no-flux condition (29a), so there is no need to subtract $\Pi^{(0)}_{xy}$ to isolate the velocity gradient information in (29b).

Imposing $\Pi_{xx} = \Pi^{(0)}_{xx}$ is equivalent to assuming that the xx component $\mu\partial_x u_x$ of the viscous stress vanishes at the wall. This is true for no-slip boundary conditions ($u_x = 0$ at the wall) and for flows with constant slip velocity. However, it is not strictly true for pressure-driven slip flows since u_x at the wall varies slowly due to slow variations in the streamwise pressure gradient, as in the analytical solution (9a)–(9c). The boundary condition (29c) should thus be considered viable when the local pressure gradient is close to constant (small Ma and Kn numbers), although in principle one could include a finite difference approximation to $\partial_x u_x$ to account for the non-equilibrium part of Π_{xx}. The density may be found from the known f_i and the imposed normal velocity, since $\rho(1-u_y) = f_0 + f_1 + f_3 + 2(f_4 + f_7 + f_8)$.

Equations (29a)-(29c) may be solved for the three unknown f_i. However, to be consistent with our second-order discretisation (24), we must impose conditions on the moments of $\overline{f}_i$. As discussed in Section IV, the conserved moments may be calculated from $\overline{f}_i$ just as easily as from f_i. The shear stress, on the other hand, must be re-expressed in terms of

$$\overline{\mathbf{\Pi}}_{xy} = \sum_i c_{ix}c_{iy}\overline{f}_i = \Pi_{xy} + \frac{\Delta t}{2\tau}\left(\Pi_{xy} - \Pi^{(0)}_{xy}\right). \tag{30}$$

Formulating the boundary conditions in terms of the barred moments determines the unknowns at the south wall as

$$\overline{f}_2 = \overline{f}_1 + \overline{f}_3 + \overline{f}_4 + 2\left(\overline{f}_7 + \overline{f}_8\right) - \rho/3 - \rho u_{slip}^2, \tag{31a}$$

$$\overline{f}_5 = -\overline{f}_1 - \overline{f}_8 + \rho/6 + \rho u_{slip}^2/2, \tag{31b}$$

$$\overline{f}_6 = -\overline{f}_3 - \overline{f}_7 + \rho/6 + \rho u_{slip}^2/2. \tag{31c}$$

The channel height is $H = (M_y - 1)\Delta x$, where M_y is the number of grid points in the vertical direction, and the relaxation time $\tau = \mu/(\rho c_s^2)$. The mean free path then becomes $\ell = KnH = \sqrt{\pi/6}\,\tau_0\rho_0/\rho$ in lattice units, where we have set $\tau = 3(\mu/\rho)\Delta t/\Delta x^2 = \tau_0\rho_0/\rho$ to keep μ constant as ρ varies. It is convenient to scale the density so that the reference density $\rho_0 = 1$. Substituting the above expressions for $\overline{f}_2$, $\overline{f}_5$, $\overline{f}_6$ into equation (30) determines

$$u_{slip} = -\frac{6\sigma\ell\left(-\overline{f}_1 + \overline{f}_3 + 2\overline{f}_7 - 2\overline{f}_8\right)}{\rho(1 + 2\tau + 6\sigma\ell)}. \tag{32}$$

Conditions on the northern wall may be found in a similar fashion. The only parameter in these boundary conditions is the same streamwise momentum accommodation coefficient σ that appears in the Navier–Maxwell boundary conditions (5) and (6) for the Navier–Stokes equations.

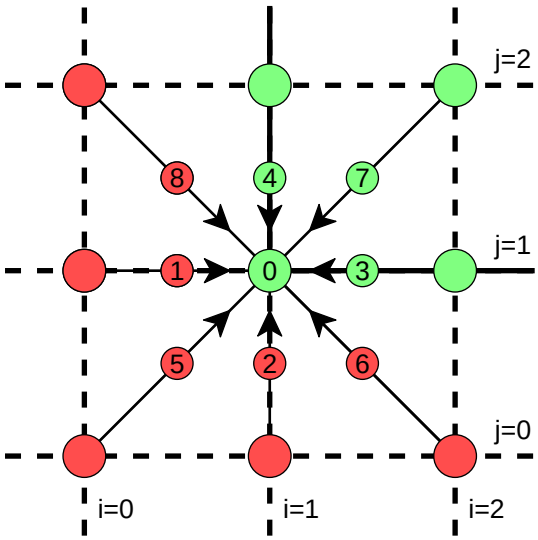

FIG. 4. (Color online) The *pre*-collisional state at the south-western corner. The five distribution functions f_1, f_2, f_5, f_6, f_8 are unknown, because the red lattice points on the lines $i = 0$ and $j = 0$ outside the boundary are missing.

Moments	Combination of unknowns
ρ, ρu_x, Π_{xx}	$f_1 + f_5 + f_8$
ρu_y, Π_{xy}, Q_{xxy}	$f_5 - f_8$
Π_{yy}, Q_{xyy}, R_{xxyy}	$f_5 + f_8$

TABLE II. Moment groups at the western boundary

B. Open boundaries and corners

To impose a (non-constant) pressure gradient along our microchannel we must apply consistent inflow and outflow conditions. Taking moments at the western open boundary (inlet), reveals the groupings of the unknown distribution functions shown in Table II. Again, we may pick one constraint from each column of the table. One possible choice is the purely hydrodynamic moments: ρ, ρu_y, and $\Pi_{yy} = P_{in} + \rho u_y^2$.

At the corners we need five constraints to determine the five unknowns shown in figure 4. Although the moments do not arrange themselves as neatly as before, we may impose the conditions from the wall and the open boundary simultaneously. The shear stress component that is required for the wall slip is determined by a combination of the four known f_i and the other hydrodynamic moments. For example, the five unknowns at the southwest corner are

$$\overline{f}_1 = 2\rho_{in}/3 - \overline{f}_0 - \overline{f}_3, \tag{33a}$$
$$\overline{f}_2 = 2\rho_{in}/3 - \overline{f}_0 - \overline{f}_4 - \rho_{in} u_{slip}^2, \tag{33b}$$
$$\overline{f}_5 = -\rho_{in}/3 + \overline{f}_0 + \overline{f}_3 + \overline{f}_4 + \overline{f}_7 + \rho_{in} u_{slip} \left(u_{slip} + 1\right)/2, \tag{33c}$$
$$\overline{f}_6 = \rho_{in}/6 - \overline{f}_7 - \overline{f}_3 + \rho_{in} u_{slip} \left(u_{slip} - 1\right)/2, \tag{33d}$$
$$\overline{f}_8 = \rho_{in}/6 - \overline{f}_7 - \overline{f}_4, \tag{33e}$$

where

$$u_{slip} = -\frac{6\sigma\ell \left(4\overline{f}_7 + \overline{f}_0 + 2\overline{f}_3 + 2\overline{f}_4 - \rho_{in}\right)}{\rho_{in}\left(1 + 2\tau + 6\sigma\ell\right)}. \tag{34}$$

C. Moment interpretation of existing boundary conditions

The grouping of moments given in Tables I and II are also convenient for analysing existing boundary conditions.[26] For example, the bounce-back scheme that sets $f_2 = f_4$, $f_6 = f_8$, $f_5 = f_7$ is equivalent to imposing the conditions

$$\rho u_y = 0, \quad Q_{xyy} = 0, \quad Q_{yyx} = 0. \tag{35}$$

This bounce-back scheme does not impose a boundary condition on the tangential velocity at the wall, given by $\rho u_x = f_1 - f_3$, but instead imposes boundary conditions on the two third-order moments that do not even appear in

the Navier–Stokes equations.[26] The "magic" combination of collision times for the $\boldsymbol{\Pi}$ and $\boldsymbol{Q}$ moments,[32]

$$\tau_Q = \frac{3}{16\tau_\Pi}, \tag{36}$$

may be interpreted as enforcing compatibility of the desired parabolic solution with the boundary conditions imposed on the components of $\boldsymbol{Q}$.[52,53] Specular reflection, on the other hand, amounts to imposing[26]

$$\rho u_y = 0, \quad \Pi_{xy} = 0, \quad Q_{xxy} = 0. \tag{37}$$

Again, no explicit boundary condition is imposed on the tangential velocity at the wall. The vanishing of the tangential momentum flux Π_{xy} precludes any transmission of stress to the wall, leading to an ever-accelerating uniform plug flow in a channel with an applied pressure difference.

Sbragaglia and Succi[23] proposed a general linear relation between the three incoming and the three outgoing distributions at a boundary. In our notation, they thus wrote f_2, f_5, f_6 as a linear combination of f_4, f_7, f_8 for the boundary shown in figure 3(a),

$$\begin{pmatrix} f_5 \\ f_2 \\ f_6 \end{pmatrix} = \begin{pmatrix} r + a/6 & a/6 & s + a/6 \\ 2a/3 & r + s + 2a/3 & 2a/3 \\ s + a/6 & a/6 & r + a/6 \end{pmatrix} \begin{pmatrix} f_7 \\ f_4 \\ f_8 \end{pmatrix}. \tag{38}$$

The three constants a, r, s satisfy $a + r + s = 1$. They may be interpreted as coefficients for the degrees of accommodation, reflection, and slip respectively in the boundary condition. In terms of moments, this boundary condition is equivalent to imposing

$$\rho u_y = 0, \quad Q_{xxy} = \frac{a}{2-a}\left(R_{xxyy} - \tfrac{1}{3}\Pi_{yy}\right) \quad Q_{xyy} = \left(\frac{1}{r + a/2} - 1\right)\Pi_{xy}, \tag{39}$$

while their simpler "slip-reflection" model with $a = 0$ and $s = 1 - r$ is equivalent to imposing

$$\rho u_y = 0, \quad Q_{xxy} = 0, \quad Q_{xyy} = (1/r - 1)\Pi_{xy}. \tag{40}$$

Again, there is no explicit boundary condition on the tangential velocity u_x, and their model was applied to a constant density flow driven by a uniform body force. This is only equivalent to a pressure-driven channel flow in the continuum limit, since it lacks the non-uniform density and non-uniform pressure gradient found in the asymptotic solution of the microchannel flow problem formulated in Sec. III.

Ansumali & Karlin[16] implemented a discrete analog of Maxwell's diffusive boundary conditions by setting

$$f_k = f_k^{(0)} \frac{f_4 + f_7 + f_8}{f_2^{(0)} + f_5^{(0)} + f_6^{(0)}}, \quad \text{for } k \in \{2, 5, 6\}, \tag{41}$$

at the south wall. Maxwell's boundary condition involves the *non-drifiting* Maxwellian; *i.e.* the equilibrium distributions in the denominator are evaluated using the density at the wall, and with the tangential velocity U_x at which the wall is moving, not the slip velocity of the fluid at the wall. In the moment basis, these conditions become

$$\rho u_y = 0, \quad Q_{xxy} = (\tfrac{1}{3} + U_x^2)\Pi_{yy} - R_{xxyy}, \quad Q_{xyy} = -\Pi_{xy} + U_x\Pi_{yy}. \tag{42}$$

The middle condition may be rewritten as $Q_{xxy} = \rho^{-1}\Pi_{yy}\Pi_{xx}^{(0w)} - R_{xxyy}$ using moments of the equilibrium $f^{(0w)}$ evaluated with the wall velocity $(U_x, 0)$.

Lee & Lin[20] used a similar boundary condition that set all distribution functions to their equilibrium values at boundary grid points, $f_k = f_k^{(0)}$ for all k. They first applied a bounce-back boundary condition, giving zero mass flux through the boundary, and then evaluated the equilibrium using the resulting density at the grid point, and the velocity of the wall. These boundary conditions have the effect of setting the normal and tangential velocities both to zero, but they obtained slip by placing their effective boundary half-way between grid points. They thus simulated a flow with a slip length equal to $\Delta x/2$.

Verhaeghe *et al.*[24] used a linear combination of the bounce-back and diffusive boundary conditions,

$$f_k = \beta f_{\overline{k}} + (1 - \beta) f_k^D, \quad k = 2, 5, 6, \quad \mathbf{c}_{\overline{k}} = -\mathbf{c}_k, \tag{43}$$

where $\beta \in [0, 1]$ and f_k^D denotes the diffusive scattering term on the right hand side of equation (41). We thus obtain a linear combination of the previous moment conditions (35) and (42),

$$\rho u_y = 0, \quad Q_{xxy} = \frac{1-\beta}{1+\beta}\left[(\tfrac{1}{3} + U_x^2)\Pi_{yy} - R_{xxyy}\right], \quad Q_{xyy} = \frac{1-\beta}{1+\beta}\left[-\Pi_{xy} + U_x\Pi_{yy}\right]. \tag{44}$$

Once again, there is no explicit constraint on the tangential velocity u_x. However, Verhaeghe *et al.*[24] eliminated the usual viscosity-dependence of the numerical slip due to the bounce-back boundary conditions by using the TRT collision operator with the "magic" relation (36) between the relaxation times for the odd and even moments. They then adjusted the parameter β so that the wall velocity in the analytical solution of their lattice Boltzmann scheme agreed with the slip given by the asymptotic solution (9a) of the Navier–Stokes equations. By contrast, our approach does not require any knowledge of an analytical solution of the lattice Boltzmann scheme, a solution that will generally not exist in more complex geometries.

VI. NUMERICAL EXPERIMENTS

Following existing literature[24] we simulate flow through a long microchannel consisting of 1001×11 grid points, for which the aspect ratio $\delta = 10^{-2}$. The density at the outlet is set to $\rho_{out} = 1$ and the dynamic viscosity is assumed constant. We therefore vary the collision time τ inversely with the local density, as described in section IV C. The accomodation constant was taken to be unity (diffuse reflection) in all simulations. Figure 5 plots the two components of velocity, normalised by $\bar{u}_o$, at the outlet when $Kn = 0.0194$. We also plot the pressure along the centerline as a function of distance along the channel. Following existing practice,[24,33] we show the scaled deviation $\delta p = (p - \bar{p}_{lin})/\bar{p}_o$ of the pressure from the linear profile $\bar{p}_{lin}(\hat{x}) = \bar{p}_o + (1-\hat{x})(\bar{p}_i - \bar{p}_o)$. This transformation makes visible the deviations from a uniform pressure gradient that arise at finite Knudsen number.

The three rows of Figure 5 correspond to three different values $\theta = 1.01$, 1.4, 2 of the ratio $\theta = \bar{p}_i/\bar{p}_o$ between the inlet and outlet pressures. When $\theta \leq 1.4$, the fractional error was observed to be around 10^{-6}. The greatest fractional error was found to be around 10^{-4} and observed for the largest Mach number. We did not run simulations with larger pressure ratios ($\theta > 2$) because our assumption that $\Pi_{xx} = \Pi^{(0)}_{xx}$ on the solid boundaries requires a negligible tangential derivative of the slip velocity. This becomes questionable when the non-linearity of the streamwise pressure gradient becomes significant. A second source of error arises when we equate the stress on the boundary with its Navier–Stokes form $\mathbf{\Pi} = \mathbf{\Pi}^{(0)} - \mu[(\nabla \mathbf{u}) + (\nabla \mathbf{u})^{\mathsf{T}}]$ to convert the Navier–Maxwell boundary condition on the strain rate to a condition on the non-equilibrium stress $\mathbf{\Pi} - \mathbf{\Pi}^{(0)}$. This approximation neglects Burnett terms of $\mathcal{O}(Kn^2)$.

Similar behavior is shown in Figure 6, for computations in which the Knudsen number $Kn = 0.194$ is an order of magnitude larger. The agreement between the analytical solutions and numerical predictions is again excellent. Increasing the Knudsen number further to $Kn = 0.388$ still shows that the discrepancy between results is very small (Figure 7), with fractional errors remaining around 10^{-5} or smaller, even though we are approaching the transition regime. However, the first order slip boundary condition (8) that forms the basis for our model is itself inaccurate when the mean free path becomes comparable to the smallest hydrodynamic length scale.[7] When $Kn = 0.388$ the Navier–Stokes solution begins to deviate noticeably from numerical solutions of the Boltzmann equation obtained using the Direct Simulation Monte Carlo (DSMC) technique,[24,33,57,58] so we did not consider $Kn > 0.388$.

To show convergence of the numerical solutions with grid refinement we compute the relative error in the three fields u, v, p using the discrete ℓ_2 norm. For example, we define the error in u by

$$\Delta u = \left(\frac{\sum_j (u_{LB}(\mathbf{x}_j) - u(\mathbf{x}_j))^2}{\sum_j u(\mathbf{x}_j)^2} \right)^{1/2}, \tag{45}$$

where $u_{LB}(\mathbf{x}_j)$ is the numerical solution, and $u(\mathbf{x}_j)$ is the asymptotic solution (9a) evaluated on the numerical grid. Figure 8 shows the errors Δu, Δv, Δp for different numbers of grid points M_y when $Kn = 0.194$, $\bar{p}_i/\bar{p}_o = 2$, and $\delta = 10^{-2}$. The convergence rates of the three different fields, u, v, p, are all approximately quadratic, as expected for our second-order lattice Boltzmann formulation.

VII. CONCLUSION

Near-continuum flows in microchannels may be described by finding solutions of the Boltzmann equation in the small Knudsen number limit using the method of matched asymptotic expansions. The flow over most of the width of the channel is described by the Navier–Stokes equations, but rapid variations of the streamwise velocity occur in $\mathcal{O}(Kn)$-wide Knudsen boundary layers at the walls, as shown in Figure 2. These Knudsen layers are essential for matching the kinetic boundary conditions applied to the Boltzmann equation at the channel walls to the effective slip velocity seen by the Navier–Stokes solution in the core. The matching conditions are given by the solution of Kramers' problem for uniform linear shear flow over a flat plate, as described in Sec. II, and the effective slip seen by the Navier–Stokes solution far from the wall is about $\sqrt{2}$ times larger than the actual slip at the wall in the solution of the Boltzmann equation.

Inspired by the kinetic origins of the lattice Boltzmann method, there have been many attempts to simulate rarefied flows in microchannels.[16–24] The vast majority of this work has implemented discrete analogs of Maxwell's combination of diffuse and specular reflecting boundary conditions for the D2Q9 lattice Boltzman method. However, the streamwise velocity profile for steady shear flows in the D2Q9 lattice Boltzmann method remains parabolic for all Knudsen numbers.[24,25] This lattice Boltzmann method thus cannot capture Knudsen layers, so a lattice Boltzmann solution computed with "correct" kinetic boundary conditions at the walls will still be erroneous in the core of the flow.

Instead, we have presented a lattice Boltzmann model implementation of slip boundary conditions for the Navier–Stokes equations, as originally formulated by Navier[43,44] and Maxwell.[12] The Navier–Stokes equations with these boundary conditions correctly capture the slip-flow regime with $0.01 \lesssim Kn \lesssim 0.1$. The overall mass flux and the velocity profile over the bulk of the channel are correct, but the velocity profile near the walls is not correct due to the absence of Knudsen layers. The effective slip velocity that must be imposed on the Navier–Stokes equations therefore differs from the tangential velocity at the wall in the solution of the Boltzmann equation, and may be determined by the solution of Kramers' problem.

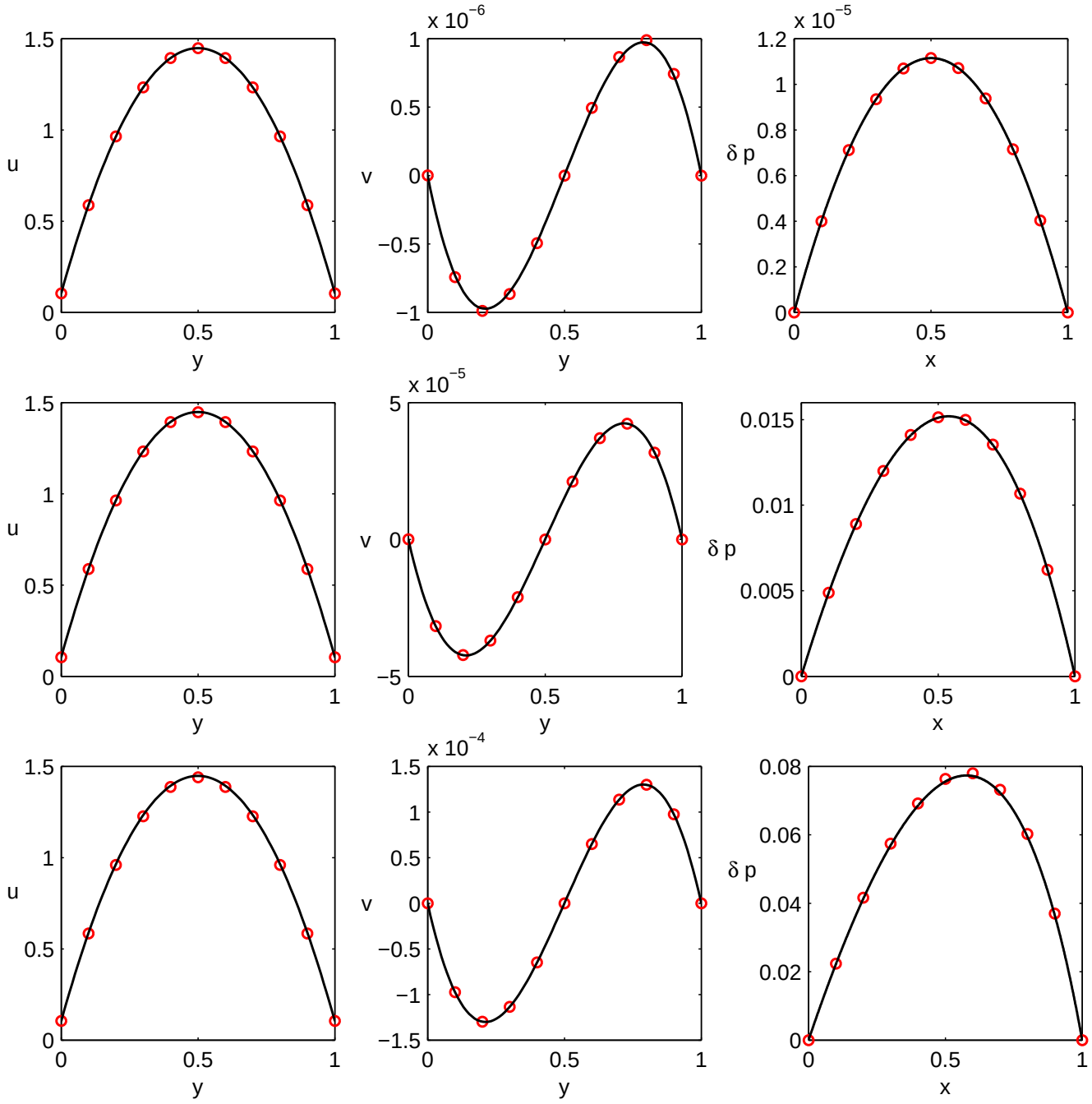

FIG. 5. (Color online) Flow through a microchannel with $\delta = 10^{-2}$ and $Kn = 0.0194$. The solid lines are the analytical solutions (9a)-(9c) and the symbols are the LB simulations. Velocity components are scaled with $\bar{u}_o$, and the centerline pressure deviation is scaled as $\delta p = (p - \bar{p}_{lin})/\bar{p}_o$. The three rows correspond to the pressure ratios $\bar{p}_i/\bar{p}_o$ =1.01, 1.4, and 2 from top to bottom.

The original form of the Navier–Maxwell boundary conditions relates the tangential slip velocity to the momentum flux at the wall. This relation fits easily into the approach of Bennett[26,27] that imposes boundary conditions directly on the moments of the distribution functions in the lattice Boltzmann equation, rather than on the distribution functions themselves. Our formulation contains only one free parameter, the same streamwise momentum accommodation coefficient σ that defines the slip length in the Navier–Maxwell boundary condition, and does not need to be calibrated against analytical solutions. Our boundary conditions impose conditions at grid points, so we avoid the numerical slip associated with bounce-back boundary conditions that place the effective boundary midway between grid points. However, our boundary conditions may also be used to impose effective no-slip boundaries at controlled locations between grid points, for which the slip length σKnH should be equated with the distance from the grid point to the boundary, as an alternative to the existing interpolated bounce-back boundary conditions.[59]

We achieve second-order accuracy by distinguishing between the f_i in the discrete Boltzmann partial differential equation and the $\overline{f}_i$ in the lattice Boltzmann equation, transforming boundary conditions imposed on moments of the f_i into conditions on the $\overline{f}_i$. We have verified our model against asymptotic solutions of the Navier-Stokes equations

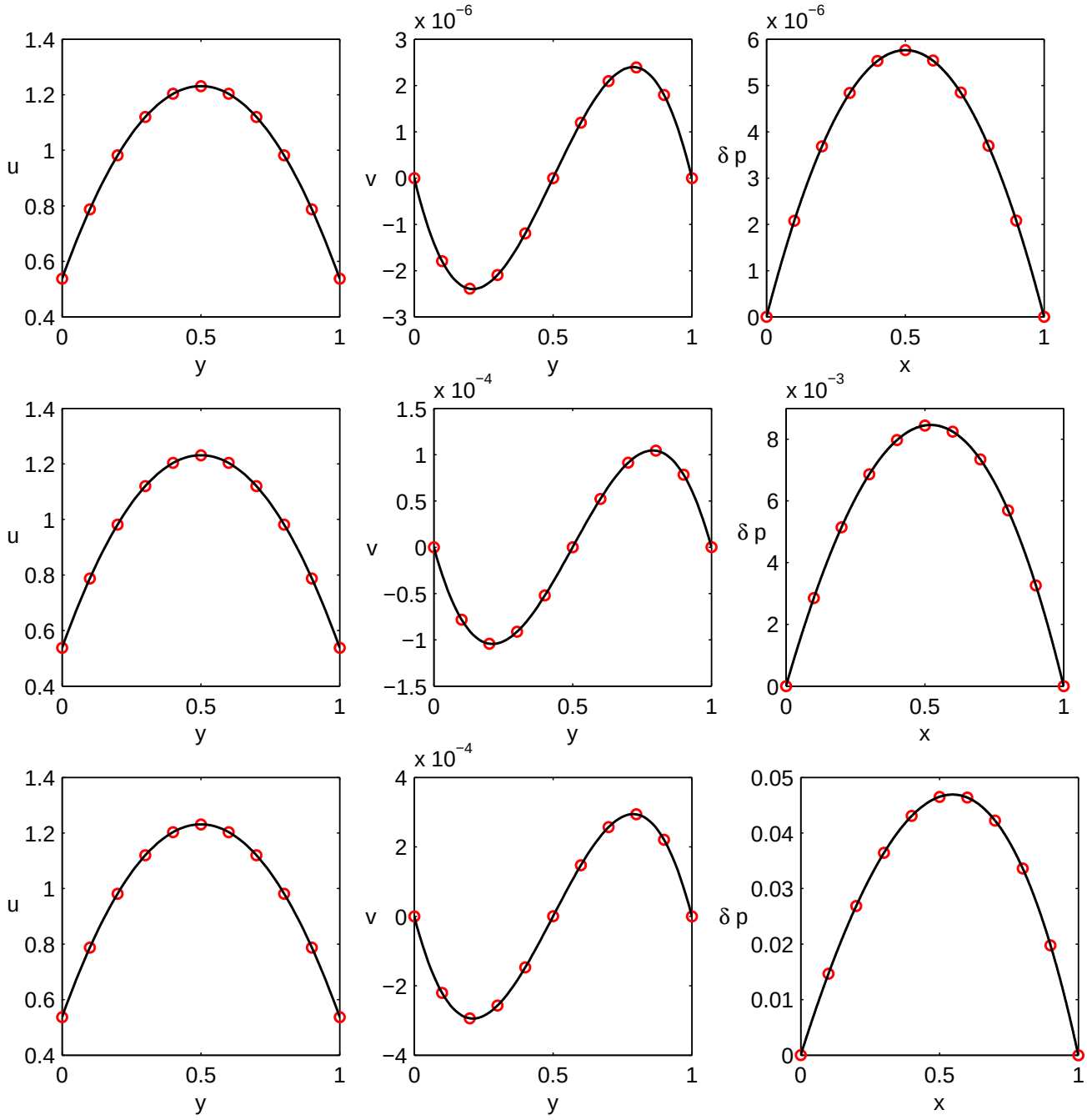

FIG. 6. (Color online) Flow through a microchannel with $\delta = 10^{-2}$ and $Kn = 0.194$. The solid lines are the analytical solutions (9a)-(9c) and the symbols are the LB simulations. Velocity components are scaled with $\bar{u}_o$, and the centerline pressure deviation is scaled as $\delta p = (p - \bar{p}_{lin})/\bar{p}_o$. The three rows correspond to the pressure ratios $\bar{p}_i/\bar{p}_o$ =1.01, 1.4, and 2 from top to bottom.

for long, thin channels, showing that our moment-based boundary conditions accurately predict the flow in the slip regime, and even match the Navier-Stokes solution up to $Kn = 0.388$, with second-order accuracy. However, at this larger Knudsen number, the Navier–Stokes solution begins to differ significantly from DSMC solutions of the Boltzmann equation.[24,33,58]

Our implementation of hydrodynamic slip boundary conditions is independent of the collision operator used, and extends easily to include the empirical second-order slip boundary conditions $u_{\|} = \sigma Kn H (1 - bKn)^{-1} \partial u_{\|} \partial n$, where b is an adjustable parameter determined from DSMC simulations.[3,60] Finally, our approach also extends to curved boundaries, and may be combined with extrapolated inflow/outflow boundary conditions (as in Ref. [24]) to give ample scope for simulating complex and practically significant flows.

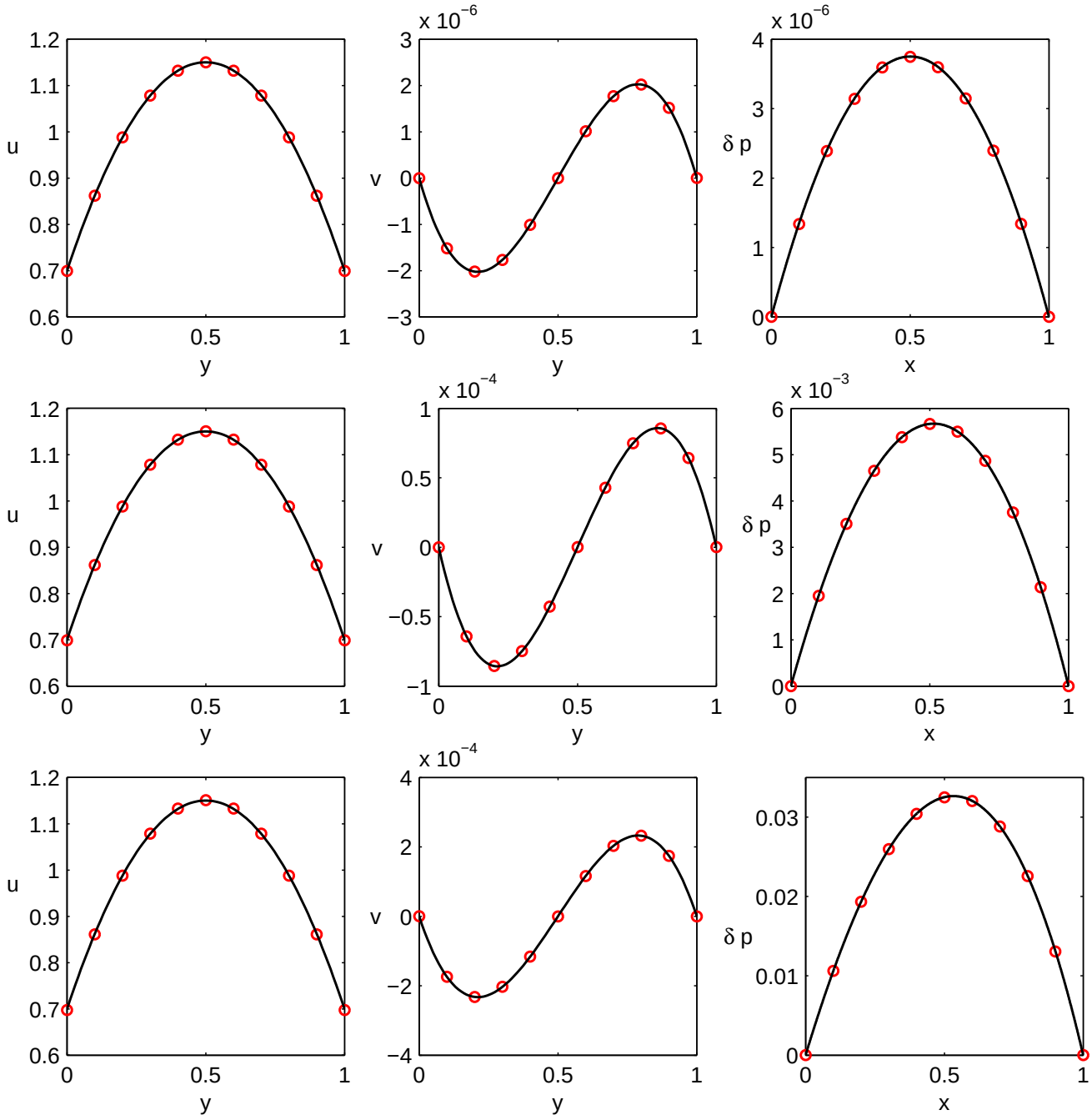

FIG. 7. (Color online) Flow through a microchannel with $\delta = 10^{-2}$ and $Kn = 0.388$. The solid lines are the analytical solutions (9a)-(9c) and the symbols are the LB simulations. Velocity components are scaled with $\bar{u}_o$. The centerline pressure deviation is scaled as $\delta p = (p - \bar{p}_{lin})/\bar{p}_o$, and is smaller than before at this larger Knudsen number. The three rows correspond to the pressure ratios $\bar{p}_i/\bar{p}_o$ =1.01, 1.4, and 2 from top to bottom.

ACKNOWLEDGMENTS

The authors thank Dr Sam Bennett for useful conversations. The authors' research is supported by Award No. KUK-C1-013-04 made by King Abdullah University of Science and Technology (KAUST); and by an Advanced Research Fellowship from the Engineering and Physical Sciences Research Council [grant number EP/E054625/1].

[1]C.-M. Ho and Y.-C. Tai, *Micro-electro-mechanical-systems (MEMS) and fluid flows*, Annu. Rev. Fluid Mech. **30**, 579 (1998).
[2]M. Gad-el Hak, *The fluid mechanics of microdevices*, ASME J. Fluid Engng. **121**, 5 (1999).
[3]G. Karniadakis, A. Beskok, and N. Aluru, *Microflows and Nanoflows* (Springer, 2005).
[4]F. Sharipov and V. Seleznev, *Data on Internal Rarefied Gas Flows*, J. Phys. Chem. Ref. Data **27**, 657 (1998).
[5]M. N. Kogan, *Kinetic theory in aerothermodynamics*, Progr. Aerospace Sci. **29**, 271 (1992).
[6]Y. Sone, *Kinetic Theory and Fluid Dynamics* (Birkhäuser, Boston, 2002).
[7]N. G. Hadjiconstantinou, *The limits of Navier–Stokes theory and kinetic extensions for describing small-scale gaseous hydrodynamics*, Phys. Fluids **18**, 111301 (2006).

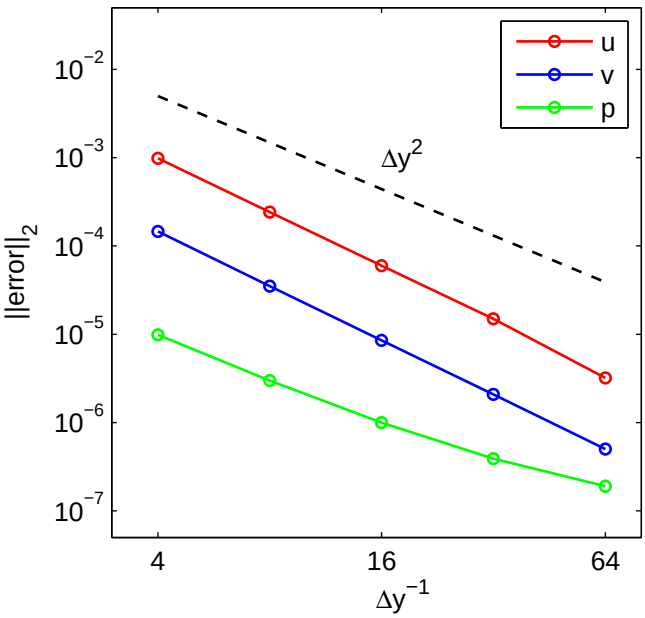

FIG. 8. (Color online) Relative errors in the ℓ_2 norm for the three quantities u, v, p for $Kn = 0.194$, $\bar{p}_i/\bar{p}_o = 2$ and varying numbers of grid points M_y across the channel. The convergence rate for both velocity components is close to second order in the grid spacing $\Delta y = H/(M_y - 1)$, while the pressure converges more slowly. The relative error in v is largest because v has much the smallest magnitude in the asymptotic solution.

[8] S. Chapman and T. G. Cowling, *The Mathematical Theory of Non-Uniform Gases* (Cambridge University Press, Cambridge, 1970), 3rd ed.

[9] C. Cercignani, *The Boltzmann Equation and its Applications* (Springer, New York, 1988).

[10] C. Cercignani, *Rarefied Gas Dynamics: From Basic Concepts to Actual Calculations* (Cambridge University Press, Cambridge, 2000).

[11] J. H. Ferziger and H. G. Kaper, *Mathematical Theory of Transport Processes in Gases* (North Holland, Amsterdam, 1972).

[12] J. C. Maxwell, *On stresses in rarified gases arising from inequalities of temperature*, Phil. Trans. Roy. Soc. Lond. **170**, 231 (1879).

[13] H. Struchtrup, *Macroscopic Transport Equations for Rarefied Gas Flows* (Springer, 2005).

[14] I. N. Ivchenko, S. K. Loyalka, and R. V. Tompson, Jr., *Analytical Methods for Problems of Molecular Transport* (Springer, 2007).

[15] T. I. Gombosi, *Gaskinetic Theory* (Cambridge University Press, Cambridge, 1994).

[16] S. Ansumali and I. V. Karlin, *Kinetic boundary conditions in the lattice Boltzmann method*, Phys. Rev. E **66**, 026311 (2002).

[17] Y. Zhang, R. Qin, Y. Sun, R. Barber, and D. Emerson, *Gas flow in microchannels – a lattice Boltzmann method approach*, J. Statist. Phys. **121**, 257 (2005).

[18] X. Nie, G. D. Doolen, and S. Chen, *Lattice-Boltzmann simulations of fluid flows in MEMS*, J. Statist. Phys. **107**, 279 (2002).

[19] C. Y. Lim, C. Shu, X. D. Niu, and Y. T. Chew, *Application of lattice Boltzmann method to simulate microchannel flows*, Phys. Fluids **14**, 2299 (2002).

[20] T. Lee and C.-L. Lin, *Rarefaction and compressibility effects of the lattice-Boltzmann-equation method in a gas microchannel*, Phys. Rev. E **71**, 046706 (2005).

[21] G. H. Tang, W. Q. Tao, and Y. L. He, *Lattice Boltzmann method for gaseous microflows using kinetic theory boundary conditions*, Phys. Fluids **17**, 058101 (2005).

[22] S. Succi, *Mesoscopic modeling of slip motion at fluid-solid interfaces with heterogeneous catalysis*, Phys. Rev. Lett. **89**, 064502 (2002).

[23] M. Sbragaglia and S. Succi, *Analytical calculation of slip flow in lattice Boltzmann models with kinetic boundary conditions*, Phys. Fluids **17**, 093602 (2005).

[24] F. Verhaeghe, L.-S. Luo, and B. Blanpain, *Lattice Boltzmann modeling of microchannel flow in slip flow regime*, J. Comput. Phys. **228**, 147 (2009).

[25] X. Y. He, Q. S. Zou, L. S. Luo, and M. Dembo, *Analytic solutions of simple flows and analysis of nonslip boundary conditions for the lattice Boltzmann BGK model*, J. Statist. Phys. **87**, 115 (1997).

[26] S. Bennett, Ph.D. thesis, University of Cambridge (2010), available from http://www.dspace.cam.ac.uk/handle/1810/226851.

[27] S. Bennett, P. Asinari, and P. J. Dellar, *A lattice Boltzmann model for diffusion of binary gas mixtures that includes diffusion slip*, Int. J. Numer. Meth. Fluids (2011), published online, doi:10.1002/fld.2549.

[28] Y.-H. Zhang, X.-J. Gu, R. W. Barber, and D. R. Emerson, *Capturing Knudsen layer phenomena using a lattice Boltzmann model*, Phys. Rev. E **74**, 046704 (2006).

[29] S. H. Kim, H. Pitsch, and I. D. Boyd, *Slip velocity and Knudsen layer in the lattice Boltzmann method for microscale flows*, Phys. Rev. E **77**, 026704 (2008).

[30] C. R. Lilley and J. E. Sader, *Velocity profile in the Knudsen layer according to the Boltzmann equation*, Proc. Roy. Soc. Lond. Ser. A **464**, 2015 (2008).

[31] P. L. Bhatnagar, E. P. Gross, and M. Krook, *A model for collision processes in gases. I. Small amplitude processes in charged and neutral one-component system*, Phys. Rev. **94**, 511 (1954).

[32] I. Ginzbourg and M. P. Adler, *Boundary flow condition analysis for the three-dimensional lattice Boltzmann model*, J. Phys. II France **4**, 191 (1994).

[33] C. Shen, D. B. Tian, C. Xie, and J. Fan, *Examination of the LBM in simulation of microchannel flow in transitional regime*, Microscale Thermophys. Eng. **8**, 423 (2004).

[34] H. A. Kramers, *On the behaviour of a gas near a wall*, Nuovo Cimento Suppl. **6**, 297 (1949).

[35] M. M. R. Williams, *A review of the rarefied gas dynamics theory associated with some classical problems in flow and heat transfer*, Z. angew. Math. Phys. **52**, 500 (2001).

[36] P. Welander, *On the temperature jump in a rarefied gas*, Arkiv Fysik **7**, 507 (1954).

[37]C. Cercignani and F. Sernagiotto, in *Rarefied Gas Dynamics*, edited by J. H. de Leeuw (Academic Press, New York, 1965), vol. 1 of *Proceedings of the Fourth International Symposium held at the Institute for Aerospace Studies, Toronto, 1964*, pp. 332–353.
[38]S. Loyalka, *Velocity profile in the Knudsen layer for the Kramer's problem*, Phys. Fluids **18**, 1666 (1975).
[39]S. Albertoni, C. Cercignani, and L. Gotusso, *Numerical evaluation of the slip coefficient*, Phys. Fluids **6**, 993 (1963).
[40]Y. Sone, C. Bardos, F. Golse, and H. Sugimoto, *Asymptotic theory of the Boltzmann system, for a steady flow of a slightly rarefied gas with a finite Mach number: General theory*, Euro. J. Mech. B **19**, 325 (2000).
[41]H. Grad, in *SIAM-AMS Proc.* (Amer. Math. Soc., Providence, R.I., 1967), vol. 1, pp. 269–308.
[42]D. A. Lockerby, J. M. Reese, D. R. Emerson, and R. W. Barber, *Velocity boundary condition at solid walls in rarefied gas calculations*, Phys. Rev. E **70**, 017303 (2004).
[43]C. L. M. H. Navier, *Mémoire sur les lois du mouvement des fluides*, Mémoires de l'Académie Royale des Sciences de l'Institut de France **VI**, 389 (1823).
[44]E. Lauga, M. P. Brenner, and H. A. Stone, in *Springer Handbook of Experimental Fluid Mechanics*, edited by C. Tropea, A. L. Yarin, and J. F. Foss (Springer, 2007), pp. 1219–1240, cond-mat/0501557.
[45]E. Arkilic, M. Schmidt, and K. Breuer, *Gaseous slip flow in long microchannels*, J. Microelectromech. Syst. **6**, 167 (1997).
[46]Y. H. Qian, D. d'Humières, and P. Lallemand, *Lattice BGK models for the Navier–Stokes equation*, Europhys. Lett. **17**, 479 (1992).
[47]X. He and L.-S. Luo, *Theory of the lattice Boltzmann method: From the Boltzmann equation to the lattice Boltzmann equation*, Phys. Rev. E **56**, 6811 (1997).
[48]X. Shan and X. He, *Discretization of the velocity space in the solution of the Boltzmann equation*, Phys. Rev. Lett. **80**, 65 (1998).
[49]P. Lallemand and L.-S. Luo, *Theory of the lattice Boltzmann method: Dispersion, dissipation, isotropy, Galilean invariance, and stability*, Phys. Rev. E **61**, 6546 (2000).
[50]D. d'Humières, I. Ginzburg, M. Krafczyk, P. Lallemand, and L.-S. Luo, *Multiple-relaxation-time lattice Boltzmann models in three dimensions*, Phil. Trans. R. Soc. Lond. A **360**, 437 (2002).
[51]P. J. Dellar, *Incompressible limits of lattice Boltzmann equations using multiple relaxation times*, J. Comput. Phys. **190**, 351 (2003).
[52]D. d'Humières and I. Ginzburg, *Viscosity independent numerical errors for Lattice Boltzmann models: From recurrence equations to "magic" collision numbers*, Comput. Math. Applic. **58**, 823 (2009).
[53]I. Ginzburg, F. Verhaeghe, and D. d'Humières, *Study of simple hydrodynamic solutions with the two-relaxation-times lattice Boltzmann scheme*, Commun. Comput. Phys. **3**, 519 (2008).
[54]X. He, X. Shan, and G. D. Doolen, *Discrete Boltzmann equation model for nonideal gases*, Phys. Rev. E **57**, R13 (1998).
[55]P. J. Dellar, *Bulk and shear viscosities in lattice Boltzmann equations*, Phys. Rev. E **64**, 031203 (2001).
[56]D. R. Noble, S. Chen, J. H. Georgiadis, and R. O. Buckius, *A consistent hydrodynamic boundary condition for the lattice Boltzmann method*, Phys. Fluids **7**, 203 (1995).
[57]G. A. Bird, *Molecular Gas Dynamics and the Direct Simulation of Gas Flows* (Clarendon Press, Oxford, 1994).
[58]C. Shen, J. Fan, and C. Xie, *Statistical simulation of rarefied gas flows in micro-channels*, J. Comput. Phys. **189**, 512 (2003).
[59]M. Bouzidi, M. Firdaouss, and P. Lallemand, *Momentum transfer of a Boltzmann-lattice fluid with boundaries*, Phys. Fluids **13**, 3452 (2001).
[60]A. Beskok and G. E. Karniadakis, *A model for flows in channels, pipes, and ducts at micro and nano scales*, Microscale Thermophys. Eng. **3**, 43 (1999).